

See discussions, stats, and author profiles for this publication at: <https://www.researchgate.net/publication/258632152>

Computational Studies of the Electronic Absorption Spectrum of [(2,2';6',2''-Terpyridine)-Pt(II)-OH] [7,7,8,8-Tetracyanoquinodimethane] Complex

ARTICLE *in* THE JOURNAL OF PHYSICAL CHEMISTRY A · NOVEMBER 2013

Impact Factor: 2.69 · DOI: 10.1021/jp408747d · Source: PubMed

CITATION

1

READS

45

3 AUTHORS, INCLUDING:



Stefan Taubert

University of Helsinki

17 PUBLICATIONS 333 CITATIONS

[SEE PROFILE](#)



Dage Sundholm

University of Helsinki

205 PUBLICATIONS 4,616 CITATIONS

[SEE PROFILE](#)

Computational Studies of the Electronic Absorption Spectrum of [(2,2';6',2"-Terpyridine)-Pt(II)-OH] [7,7,8,8-Tetracyanoquinodimethane] Complex

Hassan Rabaâ,^{†,‡} Stefan Taubert,^{‡,§,#} and Dage Sundholm*,[‡]

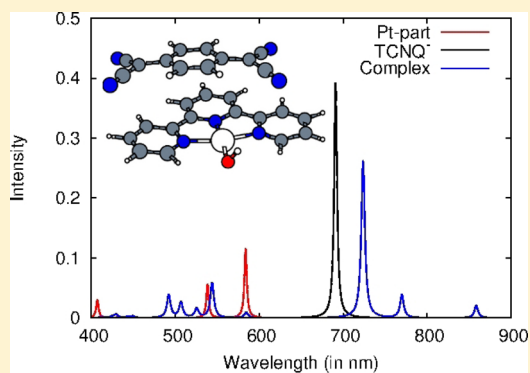
[†]Department of Chemistry, Ibn Tofail University, P.O. Box 133, Kenitra 14000, Morocco

[‡]Department of Chemistry, University of Helsinki, P.O. Box 55, A. I. Virtanens plats 1, FIN-00014 Helsinki, Finland

[§]Department of Chemistry, Aalto University, P.O. Box 16100, FIN-00076 Aalto, Finland

Supporting Information

ABSTRACT: The electronic excitation spectrum of the [(2,2';6',2"-terpyridine)-platinum(II)-OH] [7,7,8,8-tetracyanoquinodimethane] ($[\text{Pt}(\text{trpy})\text{OH}]^+ \text{TCNQ}$) complex has been studied at the linear-response approximate coupled-cluster singles and doubles (CC2) level using triple- ζ basis sets augmented with polarization functions (TZVP). The calculated ultraviolet–visible (UV–vis) spectrum of the $[\text{Pt}(\text{trpy})\text{OH}]^+ \text{TCNQ}$ complex is compared with the UV–vis spectrum measured for $[\text{Pt}(\text{tbtrpy})\text{OH}]^+ \text{TCNQ}$ ($\text{tbtrpy} = 4,4',4''-\text{Bu}_3\text{-}2,2';6',2''\text{-terpyridine}$) in dichloromethane (CH_2Cl_2) solution. The UV–vis spectrum is also compared with the calculated UV–vis spectra of $[\text{Pt}(\text{trpy})\text{OH}]^+$ and of the neutral and negatively charged TCNQ species. In contrast to previous interpretations, the CC2 calculations suggest that the $[\text{Pt}(\text{trpy})\text{OH}]^+ \text{TCNQ}$ complex is dissociated into $[\text{Pt}(\text{trpy})\text{OH}]^+$ and TCNQ^- when dissolved in CH_2Cl_2 . The computed electronic excitation energies of $[\text{Pt}(\text{trpy})\text{OH}]^+$ provide information about the charge-transfer excitations between the Pt(II) metal center and the ligands. The UV–vis spectra were also calculated at the linear-response time-dependent density functional theory (TDDFT) level using the B3LYP, BHLYP, and CAM-B3LYP functionals in combination with TZVP quality basis sets. For the TCNQ species, the TDDFT calculations yield slightly smaller excitation energies than obtained at the CC2 level, whereas for $[\text{Pt}(\text{trpy})\text{OH}]^+$ the CC2 excitation energies are slightly smaller than the TDDFT ones. For the $[\text{Pt}(\text{trpy})\text{OH}]^+ \text{TCNQ}$ complex, the B3LYP calculations yield spurious low-lying excited states rendering the spectral assignment using B3LYP data difficult. The low-energy part of the electronic excitation spectrum for the $[\text{Pt}(\text{trpy})\text{OH}]^+ \text{TCNQ}$ complex calculated at the BHLYP and CAM-B3LYP levels is reminiscent of the CC2 one because the larger amount of Hartree–Fock exchange and the long-range correction of the potential blue shifts the excitation energies.



1. INTRODUCTION

Platinum–terpyridine complexes have interesting spectroscopic properties with strong light absorption in the near-ultraviolet (UV) and short-wavelength visible (vis) regions. The absorption has been assigned to spin-allowed metal-to-ligand transitions,¹ whereas the luminescence is due to spin-forbidden phosphorescence transitions.^{1–8} Chen et al. reported that $[\text{Pt}(\text{tbtrpy})\text{X}]^+$ complexes with tbtrpy = $4,4',4''-\text{Bu}_3\text{-}2,2';6',2''\text{-terpyridine}$, ${}^t\text{Bu}$ is *tert*-butyl, X = NCS^- , OH^- , or thiolates (ArS^-), Y = Cl, OH, BF_4^- , or 7,7,8,8-tetracyanoquinodimethane (TCNQ) form supramolecular stacks in the solid state.⁹ In the solid state, the $[\text{Pt}(\text{tbtrpy})\text{X}]^+$ moiety probably donates an electron to Y forming an ionic $[\text{Pt}(\text{tbtrpy})\text{X}]^+\text{Y}^-$ complex with a formal oxidation state of Pt(II),^{9–11} because the electron affinities of TCNQ and the other Y moieties are very large.^{9,12–14} The supramolecular stacks have suitable properties for solar cell applications,^{2,6–8,10} because they strongly absorb light in a wide energy range of the visible spectrum.^{9,10} The

strong absorption is further extended to the near-infrared (NIR) region when TCNQ is used as ligand Y. The $[\text{Pt}(\text{tbtrpy})\text{X}]^+\text{TCNQ}^-$ complex is a black absorber with continuous UV–vis–NIR absorption in the whole energy range.¹⁰

Chen et al.⁹ and McMillin et al.,¹ reported that the absorption spectra of $[\text{Pt}(\text{tbtrpy})\text{X}]^+$ complexes can be understood as follows: The absorption at shorter wavelengths than 350 nm (3.5 eV) is dominated by $\pi \rightarrow \pi^*$ transitions mainly located on the tbtrpy ligand. The absorption at longer wavelengths is assigned to charge-transfer (CT) excitations from the metal to the triimine ligand and to localized excitations in the Y moiety.^{1,5,9} The tuning of the electronic

Received: September 1, 2013

Revised: November 1, 2013

Published: November 4, 2013

absorption energies of $[\text{Pt}(\text{tbtrpy})\text{X}]\text{Y}$ into the NIR region was achieved by using TCNQ.⁹

A strong absorption consisting of three bands is obtained experimentally in the low-energy region of the spectrum, ranging from 600 to 900 nm, which is typical for all $[\text{Pt}(\text{tbtrpy})\text{X}]\text{TCNQ}$ salts, because the peaks are essentially due to the absorption of the TCNQ^- anion. The absorption spectrum of $[\text{Pt}(\text{tbtrpy})\text{OH}]\text{TCNQ}$ in Figure 1 shows a broad

absorption of the TCNQ^{2-} dianion.⁹ Thus, they proposed that TCNQ^- is partially reduced to $\text{TCNQ}^{-(1+\delta)}$ and that the $[\text{Pt}(\text{trpy})\text{OH}]^+$ moiety is oxidized with the same amount.

Even though the experimental absorption spectra of $[\text{Pt}(\text{tbtrpy})\text{X}]\text{TCNQ}$ complexes have been thoroughly investigated,^{9,11} the excitation character of the involved states has not been elucidated. In this study, we employ linear-response coupled-cluster and linear-response time-dependent density functional theory calculations to provide information about the character of the electronic excitations that are responsible for the absorption peaks of the UV-vis spectra of the $[\text{Pt}(\text{trpy})\text{OH}]\text{TCNQ}$ complex, the $[\text{Pt}(\text{trpy})\text{OH}]^+$ cation, and of neutral and charged TCNQ species. The acronym trpy denotes 2,2';6',2''-terpyridine, which is a model ligand with the three *t*Bu substituents of tbtrpy replaced by hydrogens to diminish the computational requirements.

The article is outlined as follows: In the next section, the computational levels are described. In subsection 3.1, we discuss results of the electronic structure calculations on the neutral and charged TCNQ species. The absorption spectrum of the isolated $[\text{Pt}(\text{trpy})\text{OH}]^+$ is analyzed in subsection 3.2. In subsection 3.3, the calculated electronic absorption spectrum of the $[\text{Pt}(\text{trpy})\text{OH}]\text{TCNQ}$ complex is scrutinized and compared to the UV-vis spectrum measured for $[\text{Pt}(\text{tbtrpy})\text{OH}]\text{TCNQ}$ in CH_2Cl_2 solution. The obtained results are discussed in section 4. The main results of the study are summarized in section 5.

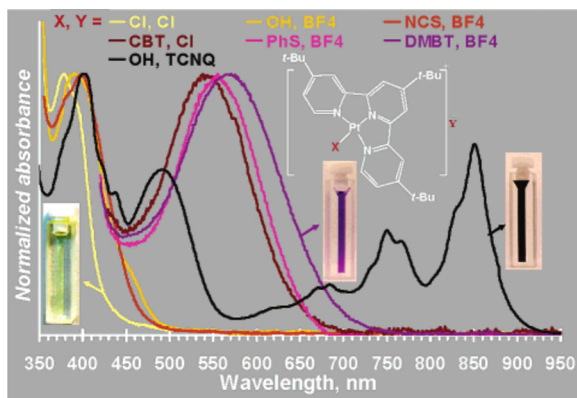


Figure 1. Experimental absorption spectra of $[\text{Pt}(\text{tbtrpy})\text{X}]\text{Y}$ complexes measured at room temperature in CH_2Cl_2 solution. Reprinted from ref 9. Copyright 2006 American Chemical Society.

peak between 450 and 550 nm with its absorption maximum at 490 nm. Chen et al. suggested that the peak at 490 nm is due to

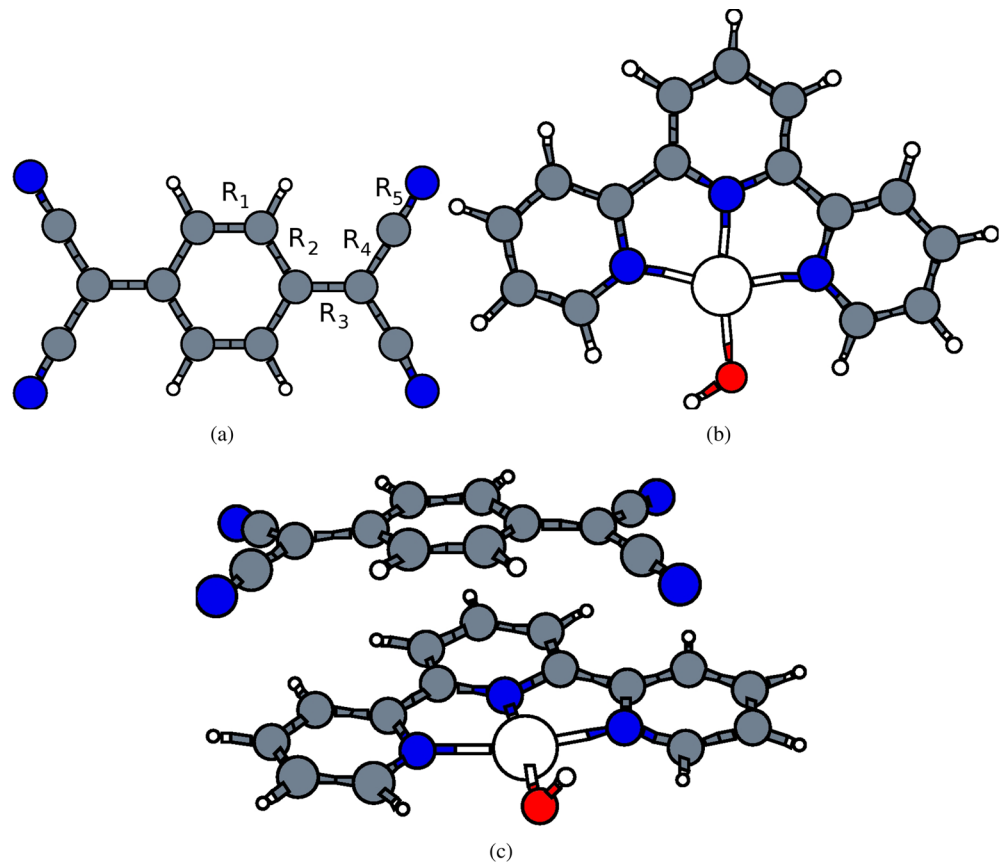


Figure 2. Molecular structures of (a) the tetracyanoquinodimethane (TCNQ) species, (b) the $[\text{Pt}(\text{trpy})\text{OH}]^+$ cation, and (c) the neutral $[\text{Pt}(\text{trpy})\text{OH}]\text{TCNQ}$ complex optimized at the B3LYP/TZVP level.

Table 1. Comparison of Calculated and Measures Bond Distances (\AA) for the TCNQ and TCNQ^- Species^a

bond	TCNQ		TCNQ^-		[Pt(trpy)OH]TCNQ	
	B3LYP	exp ⁵⁶	B3LYP	exp ⁵⁶	B3LYP	exp ⁹
R1	1.372	1.346(14)	1.370	1.361(8)	1.368(1)	1.35
R2	1.447	1.436(14)	1.421	1.419(11)	1.421(1)	1.43
R3	1.411	1.384(22)	1.426	1.414(11)	1.424(1)	1.43
R4	1.429	1.430(13)	1.412	1.419(10)	1.410(1)	1.42
R5	1.176	1.15(2)	1.160	1.16(1)	1.159(1)	1.13
Pt–N(cis)					1.949 ^b	1.96
Pt–N(trans)					2.029 ^b	2.02
Pt–N(trans)					2.040 ^b	2.04
Pt–OH					1.985 ^b	2.24
stacking					3.484 ^c	3.502

^aThe molecular structures were optimized at the B3LYP/TZVP level. The length of selected chemical bonds of the [Pt(trpy)OH]TCNQ complex are compared with experimental values. The experimental uncertainty and variations in the calculated distances are given within parentheses. ^bThe corresponding distances for [Pt(trpy)OH]⁺ are 1.947, 2.030, 2.051, and 1.970 \AA , respectively. ^cThe distance between N(cis) of [Pt(trpy)OH]⁺ and C(para) of TCNQ^- .

2. COMPUTATIONAL METHODS

The molecular structures of the studied molecules were optimized at the density functional theory (DFT) level. The DFT calculations were performed using Becke's three-parameter functional in combination with the Lee–Yang–Parr exchange–correlation functional (B3LYP).^{15,16} The Stuttgart relativistic effective core potentials were used for Pt.¹⁷ The new Karlsruhe triple- ζ basis sets augmented with polarization functions (def2-TZVP) have been used in all calculations.^{18,19} In the text, the def2 prefix is omitted for clarity. The TCNQ^{-q} ($q = 0, 1, 2$) molecules and the [Pt(trpy)OH]⁺ cation were assumed to have D_{2h} and C_s symmetry, respectively, whereas no symmetry was assumed for the [Pt(trpy)OH]TCNQ complex. The unrestricted Hartree–Fock and Kohn–Sham approaches were used for the open-shell molecules. In the optimization of the molecular structure of the [Pt(trpy)OH]TCNQ complex, Grimme's semiempirical dispersion correction was employed.²⁰ Spin singlet and doublet states were assumed for the molecules with even and odd number of electrons, respectively. The vibrational frequencies were calculated for the TCNQ molecules and for the [Pt(trpy)OH]⁺ cation. The TCNQ molecules are minima on the potential energy surface, whereas [Pt(trpy)OH]⁺ has one imaginary frequency due to the C_s symmetry constraint. The imaginary frequency corresponds to a small torsion angle of the hydroxyl (OH) group, which is a flaw that is not of relevance in this context. The vertical electronic excitation energies and oscillator strengths were calculated for the optimized ground-state structures at the approximate coupled-cluster singles and doubles (CC2) level using the resolution-of-the-identity (RI) approximation^{21–25} and at the linear-response time-dependent DFT (TDDFT) level using the B3LYP functional, Becke's half-and-half functional (BHLYP), and the CAM-B3LYP functional.^{26–32} CC2 calculations can be employed in studies of CT excitations, because the potential has the correct asymptotic long-range behavior in contrast to most density functionals.^{33,34} The UV–vis spectra were simulated by using the calculated excitation energies and oscillator strengths. Previous computational studies have shown that CC2 calculations yield accurate excitation energies and oscillator strengths for large molecules and complexes.^{35–44} In the benchmark study by Schreiber et al., the mean deviation of the CC2 singlet excitation energies from the reference values is almost as small as obtained in the

coupled-cluster calculations including triplet contributions and almost a factor of 2 better than the mean deviation obtained at the full coupled-cluster singles and doubles level.⁴³ Mulliken population analysis given as Supporting Information was obtained using the AOMix program,^{45,46} based on B3LYP/def2-TZVP calculations. B3LYP calculations using the conductor-like screening model (COSMO) with a dielectric constant (ϵ_r) for CH_2Cl_2 of 8.93 were employed to assess solvation effects.⁴⁷ Most calculations were done with Turbomole version 6.4.⁴⁸ The CAM-B3LYP calculations were performed with Gaussian 09.⁴⁹ The molecular pictures are made with XMAKEMOL.⁵⁰ The calculated spectra have been plotted with GNUPLOT.⁵¹ The orbital pictures in the manuscript are made with VMD.^{52,53} The pictures of the electron densities of the frontier orbitals in the Supporting Information have been made with GOPENMOL.^{54,55} Cartesian coordinates of the atoms are given as Supporting Information.

3. RESULTS

3.1. Tetracyanoquinodimethane Molecules.

3.1.1. TCNQ. The molecular structures of the TCNQ species shown in Figure 2a were optimized at the B3LYP level. The obtained C–C and C≡N bond distances are compared to experimental values in Table 1.⁵⁶ The first excitation energy for TCNQ of about 3.1 eV (400 nm) has been deduced from the experimental UV–vis spectrum, which has been reported in several studies.^{57–61} For neutral TCNQ, the CC2 and B3LYP calculations yield excitation energies of 3.28 eV (378 nm) and 2.83 eV (438 nm), respectively. Comparison of calculated and measured excitation energies shows that the CC2 excitation energy is somewhat larger than the experimental value, whereas the B3LYP calculations yield an excitation energy that is slightly too small as compared to experiment. The strong transition is shifted by 0.13–2.69 eV (461 nm) when solvent effects are considered at the COSMO level. The CC2 and the B3LYP values agree reasonably well with experiment,^{57–61} because vibrational effects can be of the same size as the deviation between calculated and measured excitation energies. The calculated excitation energy is expected to be slightly larger than the experimental value, because the experimental UV–vis spectrum for TCNQ was measured in acetonitrile solution,⁶¹ whereas the calculations have been performed on a single isolated TCNQ molecule. Dierksen and Grimme estimated that the solvent red shifts the excitation energy by 0.15 eV.⁶² With

this correction, the CC2 excitation energy of 3.13 eV (396 nm) agrees almost perfectly with experiment. The second excited state is less relevant in this context because it lies more than 5 eV above the ground state according to the CC2 calculation and the measured UV-vis spectrum.^{60,61} The calculated and measured excitation energies and oscillator strengths for TCNQ are compared in Table 2. Only the excited states that

Table 2. Lowest Excitation Energies (E , eV) and Oscillator Strengths (f) of Neutral TCNQ Calculated at the CC2, B3LYP, and CAM-B3LYP Levels Using the TZVP Basis Set^a

state	CC2		B3LYP		CAM-B3LYP		exp^{60}
	E	f	E	f	E	f	
1B _{2u}	3.28	1.339	2.83	1.014	2.94	1.129	3.14 ^b
1B _{1u}	5.61	0.003	4.40	0.000	5.06	0.000	5.25
1B _{3u}	5.97	0.106	4.75	0.079	5.54	0.100	

^aThe first peak maximum of the experimental UV-vis spectrum of TCNQ measured in acetonitrile solution appears at 3.17 eV.⁶¹ ^bThe first excitation energy calculated at the CASPT2/aug-cc-pVDZ level is 3.02 eV.⁶³

can be reached by dipole-allowed transitions are considered in this study. The UV-vis spectrum simulated using CC2 excitation energies and oscillator strengths is shown in Figure 3a. The excitation energies calculated at the CC2 and B3LYP levels are also in good agreement with the value of 3.02 eV (411 nm) obtained in complete active space second-order perturbation theory (CASPT2) calculations.⁶³

3.1.2. TCNQ^{2-} . The experimental UV-vis spectrum for the TCNQ^{2-} dianion recorded in acetonitrile solution yielded an excitation energy of 2.56 eV (484 nm) for the first excited state,⁵⁷ which can be compared to the CC2 and B3LYP values of 4.17 eV (297 nm) and 3.94 eV (315 nm), respectively. Repeating the CC2 calculation using Dunning's triple- ζ basis sets augmented with diffuse functions (aug-cc-pVTZ)⁶⁴ yields a

value of 2.61 eV (476 nm) for the first excited state, which is in very good agreement with the experimental value of 2.56 eV (484 nm).⁵⁷ However, the detection of the state might be hard due to its very small oscillator strength of 0.005. The strong transition to the 2B_{2u} state has an energy of 3.95 eV (314 nm), which does not deviate much from the energy of 4.17 eV (297 nm), which was obtained for the strong transition in the CC2/TZVP calculations. The position of the strong transition is red-shifted by only 0.005 eV when solvent effects are considered at the COSMO level. The calculated excitation energies and oscillator strengths for the TCNQ^{2-} dianion are compared to experimental values in Table 3. The UV-vis spectrum for the TCNQ^{2-} dianion obtained using the CC2/TZVP excitation energies and oscillator strengths (intensities) is depicted in Figure 3b.

Table 3. Lowest Excitation Energies (E , eV) and the Oscillator Strengths (f) of the TCNQ^{2-} Dianion Calculated at the CC2/TZVP, CC2/aug-cc-pVTZ, and B3LYP/TZVP Levels Compared to Experimental Values

state	CC2/TZVP		CC2/aug-cc-pV-TZ ^a		B3LYP/TZVP		exp^{57}
	E	f	E	f	E	f	
1B _{2u}	4.17	0.967	3.41	0.025	3.94	0.780	2.56
1B _{1u}	4.38	0.000	2.61	0.005	3.71	0.000	3.30
2B _{1u}	5.03	0.001	3.36	0.000	4.80	0.002	3.69
1B _{3u}	3.54	0.003	3.42	0.007	3.28	0.002	

^aThe energy and oscillator strength of the strong B_{2u} state (the fifth state) are 3.95 eV and 0.611, respectively.

A fair comparison between calculated and measured excitation energies for the dianion is complicated as the measurement was performed in acetonitrile solution, whereas isolated molecules have been investigated in this study. For an isolated molecule in the gas phase, the wave function of the

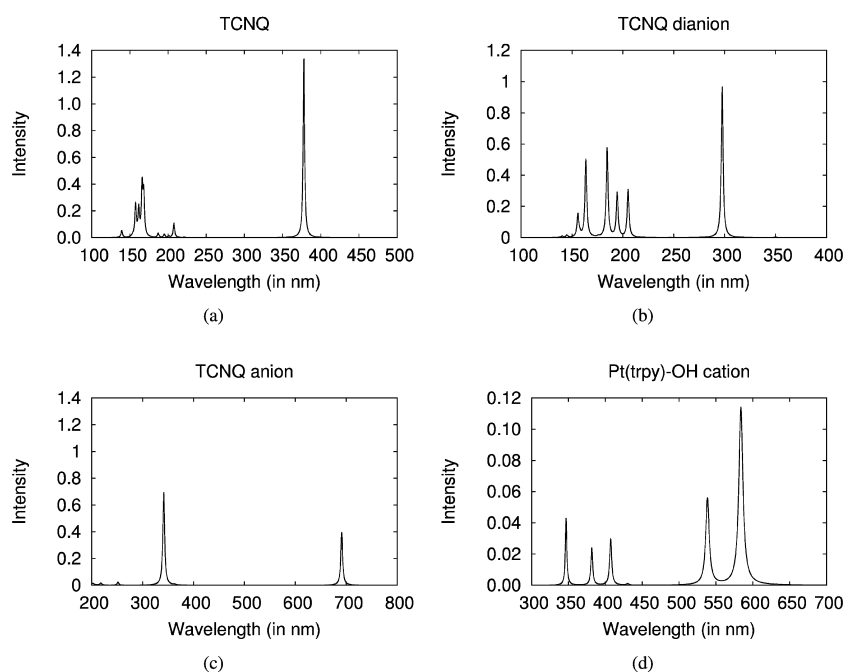


Figure 3. Simulated UV-vis spectra of (a) neutral TCNQ, (b) the TCNQ^{2-} dianion, (c) the TCNQ^{-} anion, and (d) the $[\text{Pt}(\text{trpy})\text{OH}]^+$ cation. The CC2/TZVP excitation energies and oscillator strengths used for the spectra are given in Tables 2–5, respectively.

Table 4. Lowest Excitation Energies (E , eV) and Oscillator Strengths (f) of the TCNQ^- Anion Calculated at the CC2, B3LYP, and CAM-B3LYP Levels Using the TZVP Basis Set^a

state	CC2		B3LYP		CAM-B3LYP		E
	E	f	E	f	E	f	
1B _{2u}	1.79	0.393	1.78	0.293	1.70	0.386	1.46 (1.62) ^{a,b}
2B _{2u}	3.63	0.691	3.51	0.565	3.50	0.006	3.14 ^b
3B _{2u}	4.93	0.021	4.43	0.059	3.59	0.459	5.25
1B _{1u}	4.79	0.000	4.02	0.000	4.49	0.132	
2B _{1u}	5.61	0.000	4.73	0.000	5.01	0.002	
3B _{1u}	5.87	0.001	4.83	0.000	5.45	0.000	
1B _{3u}	3.42	0.005	3.18	0.003			
2B _{3u}	5.69	0.014	4.65	0.001			

^aThe energy of the first excited state calculated at the B3LYP/(5s3p1d/3s1p) level is 1.78 eV and the corresponding 0–0 transition energy is 1.62 eV.⁶² ^bThe two lowest excitation energies at the CASPT2/aug-cc-pVDZ level are 1.52 and 2.71 eV.⁶³ ^cExperimental peak maxima of TCNQ^- measured in acetonitrile solution appear at 1.47 and 1.63 eV as well as a broad peak in the range of 2.8–3.5 eV.^{57,61}

dianion is very diffuse, whereas the surrounding solvent molecules stabilize the dianion and restrict the orbital extension. Thus, the solvent might change the order of the excited states and affect the intensities of the transitions.

3.1.3. TCNQ^- . In the energy range below 2 eV (620 nm), the UV-vis spectrum of the TCNQ^- anion measured in acetonitrile consists of three peaks with fine structure. The three peak maxima appear at 1.47 eV (843 nm), 1.63 eV (761 nm), and 1.83 eV (678 nm).^{60,61} A broad peak appears between 2.76 eV (450 nm) and 3.54 eV (350 nm).⁶¹ The CC2 and B3LYP calculations show that TCNQ^- has only one dipole-allowed ground-state transition in the low-energy region. The simulated electronic excitation spectrum is shown in Figure 3c, and the corresponding excitation energies are listed in Table 4. The CC2 excitation energies of the two lowest excited states are 1.79 eV (693 nm) and 3.63 eV (342 nm), respectively, as compared to the corresponding B3LYP energies of 1.78 eV (697 nm) and 3.51 eV (353 nm). The two strongest bands in Table 4 are red-shifted by 0.05 and 0.03 eV, respectively, when solvent effects are considered at the COSMO level. Because only one electronic transition is obtained in the CC2 and B3LYP calculations, the splitting into the three peaks with fine structure in the low-energy part of the spectrum must be due to vibrational coupling, which agrees with the previous interpretation based on computed excitation energies.^{62,65}

At the B3LYP level, Dierksen and Grimme obtained a vertical excitation energy of 1.78 eV (697 nm) for TCNQ^- in the gas phase.⁶² By considering zero-point vibrational corrections, they obtained a 0–0 transition of 1.62 eV (765 nm), which was in excellent agreement with experiment after they corrected the experimental value with 0.15 eV due to solvent effects. The CC2 and B3LYP excitation energies are somewhat larger than the excitation energies of 1.52 eV (816 nm) and 2.71 eV (458 nm) calculated at the CASPT2 level for the two lowest states of TCNQ^- .⁶³

3.2. $[\text{Pt}(\text{trpy})\text{OH}]^+$ Cation. The molecular structure of the $[\text{Pt}(\text{trpy})\text{OH}]^+$ cation shown in Figure 2b was optimized at the B3LYP level. The excitation energies for $[\text{Pt}(\text{trpy})\text{OH}]^+$ calculated at the CC2 level largely agree with the B3LYP ones. However, the B3LYP calculations yielded excitation energies that are 0.1–0.5 eV larger than the CC2 ones. Usually, the B3LYP excitation energies are somewhat smaller than those obtained at the CC2 level. The D_1 diagnostic value of 0.074 obtained at the second-order Møller–Plesset level is somewhat larger than the generally recommended maximum value of 0.05. The D_1 value indicates a trifle multireference character of the

ground state as also obtained for the $[\text{Pt}(\text{trpy})\text{OH}]\text{TCNQ}$ complex. The B3LYP excitation energies are somewhat too large as compared to the excitation energies deduced from the measured UV-vis spectra of the $[\text{Pt}(\text{tbtrpy})\text{Y}]$ complexes with Y^- anions that do not absorb in the visible range of the spectrum.⁹ The excitation energies calculated using the CAM-B3LYP functional are much larger than the ones obtained at the B3LYP and CC2 levels of theory and also too large as compared to values deduced from experimental UV-vis spectra. The CC2 excitation energies show a better agreement with experimental values than the values obtained using TDDFT calculations. The comparison with experiment is not completely unproblematic, because solvent effects and the interaction between the $[\text{Pt}(\text{tbtrpy})\text{X}]^+$ cation and Y^- anions might cause significant shifts in the transition energies.⁹ In the B3LYP-COSMO calculations, the two lowest states are blue-shifted by 0.24 and 0.37 eV, respectively, as compared to the gas-phase calculation. The excitation energies and oscillator strengths calculated at the CC2, B3LYP, and CAM-B3LYP levels are compared in Table 5. The UV-vis spectrum simulated using the CC2 data is shown in Figure 3d.

According to the CC2 calculations, the lowest excitation energy of the $[\text{Pt}(\text{trpy})\text{OH}]^+$ cation is 2.12 eV (585 nm). The ground-state transition to the first excited state is the strongest one with an oscillator strength of 0.114. Two other excited states with relatively large oscillator strengths appear in the visible range of the UV-vis spectrum, namely at 2.30 eV (539

Table 5. Lowest Excitation Energies (E , eV) and Oscillator Strengths (f) of the $[\text{Pt}(\text{trpy})\text{OH}]^+$ Cation Calculated at the CC2, B3LYP, and CAM-B3LYP Levels Using the TZVP Basis Set

state	CC2		B3LYP		CAM-B3LYP	
	E	f	E	f	E	f
2A'	2.12	0.114	2.54	0.038	3.06	0.036
3A'	2.30	0.055	2.59	0.027	3.40	0.045
4A'	3.05	0.030	3.23	0.002	3.66	0.000
5A'	3.25	0.024	3.50	0.005	4.39	0.296
6A'	3.58	0.043	3.65	0.001	4.41	0.102
1A''	2.88	0.001	3.01	0.001	3.51	0.003
2A''	3.04	0.000	3.40	0.000	4.00	0.000
3A''	3.15	0.000	3.47	0.000	4.02	0.000
4A''	3.34	0.000	3.85	0.000	4.29	0.000
5A''	4.03	0.000	3.92	0.000	4.80	0.000

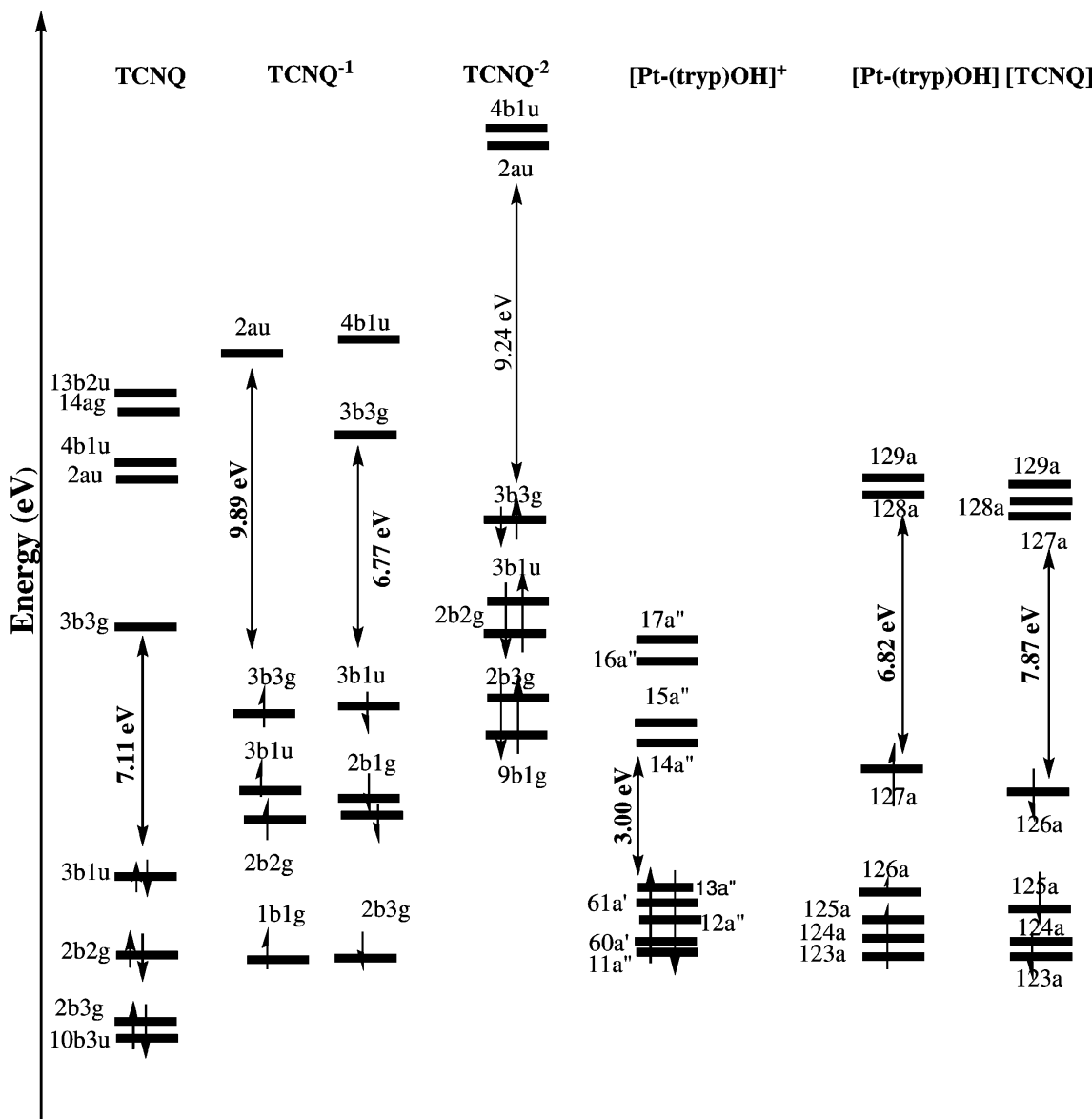


Figure 4. Orbital energy levels for TCNQ, TCNQ⁻, TCNQ²⁻, [Pt(trpy)OH]⁺, and the [Pt(trpy)OH]TCNQ complex are shown. The picture has been made with CHEMDRAW.

nm) and 3.05 eV (407 nm). The excited state at 2.88 eV (431 nm), which has a very small oscillator strength of 0.001, can probably not be assigned in the recorded UV-vis spectrum.⁹

The broad peak appearing at 500 nm in the experimental UV-vis spectra of [Pt(tbtrpy)X]Y measured in CH₂Cl₂ must be assigned to the [Pt(tbtrpy)X] moiety, because the band appears for all the studied [Pt(tbtrpy)X]Y species regardless of the counterion.⁹ The best candidates responsible for the transition are the two lowest excited states of [Pt(tbtrpy)OH]⁺ at 2.12 eV (585 nm) and 2.30 eV (539 nm), which have oscillator strengths of 0.114 and 0.055, respectively. The higher excited states contribute to the absorption band at about 400 nm. The orbital energies of the frontier orbitals calculated at the Hartree-Fock level are shown in Figure 4. The dominating excitation contributing to the lowest excited state of [Pt(trpy)-OH]⁺ is 12a'' → 14a'', i.e., from HOMO-1 to LUMO. HOMO denotes the highest occupied molecular orbital and LUMO is the lowest unoccupied molecular orbital.

The orbital plots in Figure 5 show that the HOMO-1 orbital of [Pt(trpy)OH]⁺ has a significant π character located on the trpy ligand and on the OH ligand. LUMO has a significant electron density on trpy and on Pt, but it contributes less to the electron density on the hydroxyl group, implying that the first excited state has a smaller density on the OH ligand and a larger density on Pt as compared to densities of the ground state. Thus, the HOMO-1 → LUMO excitation causes a charge transfer from OH and Pt to trpy. The second excited state is dominated by 12a'' → 15a'', i.e., from HOMO-1 to LUMO+1. LUMO+1 is a trpy π orbital. Thus, the excitation moves electrons from OH to the trpy ligand. The broad peak at 500 nm seems to be a CT excitation that moves electrons from ligand X to Pt and to the trpy ligand.

3.3. [Pt(trpy)OH]TCNQ Complex. **3.3.1. Molecular Structure.** The molecular structure of the [Pt(trpy)OH]TCNQ complex optimized at the B3LYP level is shown in Figure 2c. In Table 1, selected bond distances of the [Pt(trpy)OH]TCNQ complex are compared to experimental data. The bond lengths

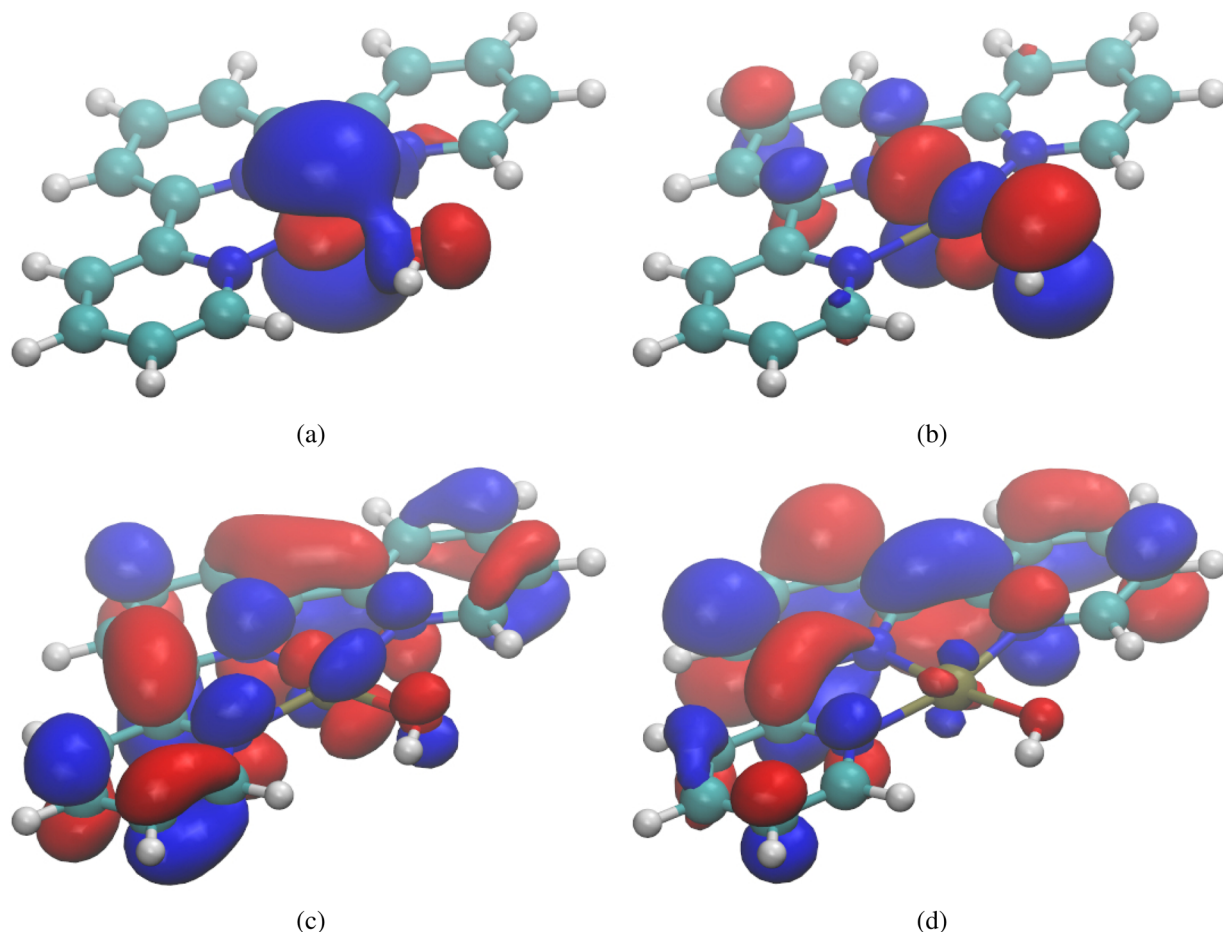


Figure 5. HOMO-1 (a), HOMO (b), LUMO (c), and LUMO+1 (d) orbitals of the $[\text{Pt}(\text{trpy})\text{OH}]^+$ cation.

Table 6. Lowest Excitation Energies (E , eV) and Oscillator Strengths (f) of the Neutral $[\text{Pt}(\text{trpy})\text{OH}]\text{TCNQ}$ Complex calculated at the CC2, B3LYP, BHLYP, and CAM-B3LYP Levels Using the TZVP Basis Set

state	CC2		B3LYP		BHLYP		CAM-B3LYP	
	E	f	E	f	E	f	E	f
2A	1.44	0.020	1.01	0.014	1.53	0.272	1.58	0.245
3A	1.61	0.038	1.23	0.005	1.90	0.011	1.85	0.010
4A	1.71	0.260	1.56	0.111	2.14	0.002	2.12	0.002
5A	2.12	0.009	1.86	0.057	2.27	0.002	2.37	0.001
6A	2.28	0.058	1.95	0.001	2.48	0.013	2.49	0.011
7A	2.36	0.015	2.03	0.004	2.70	0.002	2.74	0.004
8A	2.45	0.026	2.27	0.003	2.81	0.003	2.93	0.000
9A	2.51	0.004	2.34	0.001	2.94	0.000	2.97	0.001
10A	2.52	0.035	2.41	0.008	3.09	0.000	3.07	0.002
11A	2.76	0.003	2.49	0.021	3.45	0.011	3.13	0.020
12A	2.80	0.002	2.57	0.002	3.46	0.125	3.34	0.001
13A	2.89	0.006	2.62	0.011	3.47	0.012	3.35	0.000
14A	2.92	0.002	2.69	0.010	3.53	0.010	3.36	0.003
15A	2.97	0.001	2.70	0.015	3.55	0.000	3.41	0.003
16A	3.01	0.001	2.71	0.003	3.60	0.000	3.50	0.008
17A			2.81	0.000	3.63	0.001	3.51	0.049
18A			2.85	0.000	3.66	0.004	3.53	0.000
19A			2.89	0.000	3.69	0.007	3.55	0.005
20A			2.97	0.003	3.72	0.002	3.57	0.089
21A			3.00	0.003	3.77	0.023	3.62	0.071

of the TCNQ moiety are also compared to calculated bond distances for the TCNQ and TCNQ^- species. The TCNQ bonds are labeled in Figure 2a.

The calculated Pt–N distances of the $[\text{Pt}(\text{trpy})\text{OH}]^+$ moiety are in excellent agreement with experimental values, whereas the obtained Pt–OH distance is 0.25 Å shorter than the X-ray

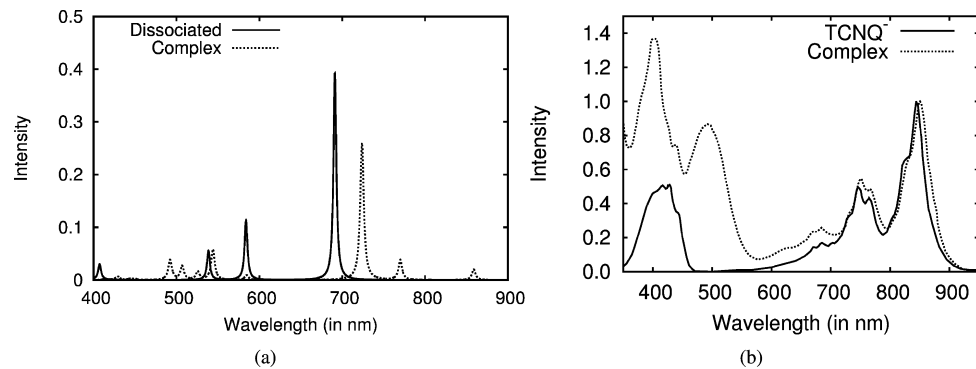


Figure 6. (a) Comparison of the UV-vis spectrum for the $[\text{Pt}(\text{trpy})\text{OH}]\text{TCNQ}$ complex with the combined spectra of noninteracting $[\text{Pt}(\text{trpy})\text{OH}]^+$ and TCNQ^- ions calculated at the CC2 level. The CC2/TZVP excitation energies and oscillator strengths used for the $[\text{Pt}(\text{trpy})\text{OH}]\text{TCNQ}$ are given in Table 6. (b) Comparison of the experimental spectra for $[\text{Pt}(\text{trpy})\text{OH}]\text{TCNQ}$ and TCNQ^- measured in CH_2Cl_2 and acetonitrile, respectively.^{9,61}

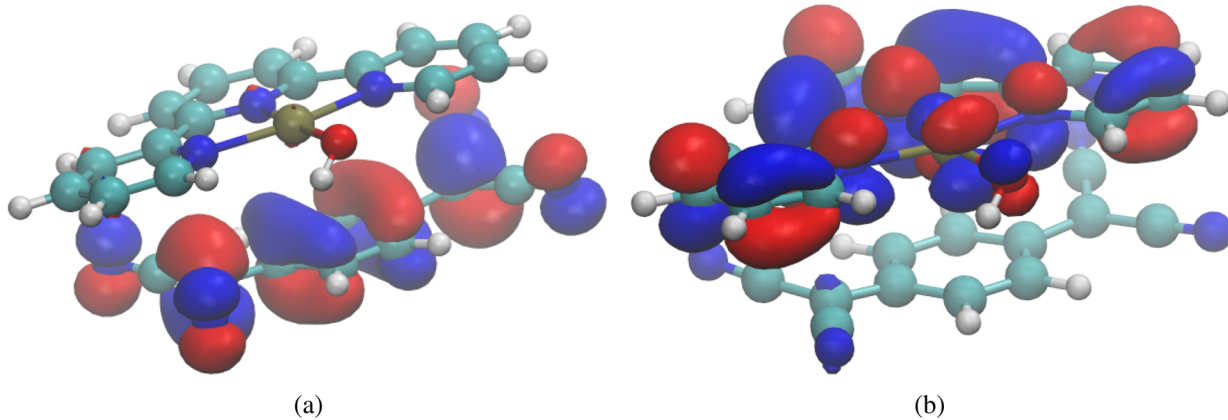


Figure 7. HOMO (a) and α LUMO (b) of the $[\text{Pt}(\text{trpy})\text{OH}]\text{TCNQ}$ complex.

value. The large discrepancy between calculated and measured Pt–OH distances is not completely understood. However, it might be due to interactions with neighboring molecules in the solid state, because the experimental Pt–O distance is unusually long.⁶⁶

Comparison of the calculated bond lengths for the TCNQ moiety of the $[\text{Pt}(\text{trpy})\text{OH}]\text{TCNQ}$ complex with calculated bond distances of TCNQ and TCNQ^- reveals that the complex is completely ionic, because all calculated C–C bond lengths for the TCNQ moiety are in perfect agreement with those calculated for the TCNQ^- anion. The $[\text{Pt}(\text{trpy})\text{OH}]^+\text{TCNQ}^-$ character is also confirmed by Mulliken population analysis. The Mulliken charges are given as Supporting Information. Ground-state calculations at the B3LYP level using COSMO to simulate the CH_2Cl_2 solvent yielded a lower energy for a mixture of charged TCNQ^- and $[\text{Pt}(\text{trpy})\text{OH}]^+$ species than for neutral TCNQ and $[\text{Pt}(\text{trpy})\text{OH}]$ molecules in the CH_2Cl_2 solution. The spin contamination of the open-shell complex is not severe as the expectation value of S^2 is 0.76 for the doublet state.

3.3.2. Calculated UV-Vis Spectrum. The vertical electronic excitation energies calculated at the B3LYP, BHLYP, CAM-B3LYP, and CC2 levels are listed in Table 6. The UV-vis spectra in Figure 6a are simulated using the CC2 excitation energies and oscillator strengths. The experimental spectra for $[\text{Pt}(\text{trpy})\text{OH}]\text{TCNQ}$ and TCNQ^- are shown for comparison in Figure 6b.^{9,61} The first excitation energy calculated at the CC2 level is 1.44 eV (861 nm). However, this transition is

difficult to deduce from the experimental spectrum due to the very small oscillator strength of 0.020. The first excited state is a CT state that is dominated by the excitation of an α electron in $127a_{\alpha}$ (HOMO) to $128a_{\alpha}$ (α LUMO). α LUMO is the first virtual π_{α} orbital, which is located on the trpy ligand. The HOMO and α LUMO are depicted in Figure 7. The orbital labels are given in the molecular orbital energy diagram in Figure 4. The electron densities of orbitals in the vicinity of the frontier orbitals are given as Supporting Information.

The second excited state at 1.61 eV (770 nm) has an oscillator strength of 0.038. It corresponds to a CT excitation from the $127a_{\alpha}$ orbital located on TCNQ^- to $129a_{\omega}$, which is a π_{α} orbital of the trpy ligand. The third excited state at 1.71 eV (725 nm) has a large oscillator strength of 0.260. It is also a CT transition that is dominated by the excitation from $126a_{\beta}$ to $127a_{\beta}$ on TCNQ^- with significant contributions from $126a_{\beta}$ to $128a_{\beta}$ and $126a_{\beta}$ to $129a_{\beta}$ excitations, where $128a_{\beta}$ and $129a_{\beta}$ are π_{β} orbitals of the trpy ligand.

The excitation at 2.12 eV (585 nm) involves transitions from $123a_{\beta}$ to $127a_{\beta}$ and from $124a_{\beta}$ to $127a_{\beta}$, which is the β LUMO orbital located on TCNQ^- . The $123a_{\beta}$ orbital is located on Pt and OH and $124a_{\beta}$ is distributed over the whole complex. Thus, the excitation at 2.12 eV (585 nm) is partially a CT state that increases the negative charge on TCNQ^- by moving electrons from $[\text{Pt}(\text{trpy})\text{OH}]^+$ toward TCNQ^- .

The largest orbital excitation contribution to the excited state at 2.28 eV (544 nm) is the $125a_{\alpha}$ to $128a_{\alpha}$ transition, which is an excitation of charge-transfer metal to ligand (CTML) type.

Orbital $125a_1$ contributes to the electron density at Pt and OH, but it has also a significant π orbital contribution on TCNQ^- , whereas $128a_1$ is a trpy π orbital. The excitation at 2.28 eV (544 nm) is thus mainly a Pt–X to trpy CT excitation. However, it has also a significant component of the CT from TCNQ^- to $[\text{Pt}(\text{trpy})\text{OH}]^+$. The excitation character of the weak transitions at 2.36 eV (525 nm) and 2.45 eV (506 nm) and of the higher excited states is hard to elucidate, because the transition involves many orbitals in the vicinity of the frontier orbitals. The higher excited states have small oscillator strengths rendering the experimental assignment difficult.

For the $[\text{Pt}(\text{trpy})\text{OH}]\text{TCNQ}$ complex, the B3LYP calculations of the electronic excitation energies yielded low-lying states with the first excited state at 1.01 eV (1228 nm) having an oscillator strength of 0.014. The lowest state seems to be the same CT state as obtained as the lowest excited state in the CC2 calculation with an excitation energy that is 0.37 eV smaller than the CC2 one. The B3LYP energies of the CT excitations are smaller than the corresponding excitation energies calculated at the CC2 level because of the incorrect asymptotic shape of the long-range DFT potential.³³ The second transition at the B3LYP level corresponds to the second excited state of the CC2 calculation. It is also a CT transition resulting in an excitation energy that is 0.28 eV smaller than the CC2 one. The third and the fourth states at 1.56 eV (795 nm) and 1.86 eV (667 nm), respectively, involve excitations in the TCNQ^- moiety as well as contributions due to CT excitations from TCNQ^- to $[\text{Pt}(\text{trpy})\text{OH}]^+$. For the $[\text{Pt}(\text{trpy})\text{OH}]\text{TCNQ}$ complex, the B3LYP excitation energies are generally smaller than the ones calculated at the CC2 level, due to the CT character of the transitions, which renders comparisons to experiment difficult. The energies of the lowest excited states calculated at the B3LYP level are significantly blue-shifted when solvent effects are considered using COSMO. The excitation energy of the first excited state at the B3LYP-COSMO level is 1.57 eV (790 nm). The energy of the second excited state, which is the first strong transition, is 1.64 eV (757 nm). The excitation energies calculated at the B3LYP-COSMO level are given as Supporting Information. For the $[\text{Pt}(\text{trpy})\text{OH}]^+$ cation, the CC2 excitation energies are smaller than those obtained at the B3LYP level, because of a trifle multireference character of the ground state. The ground state of the $[\text{Pt}(\text{trpy})\text{OH}]\text{TCNQ}$ complex has about the same extent of multireference character as the $[\text{Pt}(\text{trpy})\text{OH}]^+$ cation, implying that the same accuracy can be expected for the CC2 excitation energies of $[\text{Pt}(\text{trpy})\text{OH}]^+$ and $[\text{Pt}(\text{trpy})\text{OH}]\text{TCNQ}$.

Calculations employing the BHLYP and CAM-B3LYP functionals yield practically identical excitation energies and oscillator strengths for the states in the visible range. The energy of the lowest excited state of 1.58 eV (785 nm) obtained at the CAM-B3LYP level is 0.12 eV smaller than the energy of the strong band of TCNQ^- , whereas for TCNQ^- and the $[\text{Pt}(\text{trpy})\text{OH}]\text{TCNQ}$ complex the experimental absorption spectra corresponding to the first strong transition are identical (Figure 6b), which suggests that the complex is indeed dissociated in the CH_2Cl_2 solution. The experimental spectra are slightly shifted because they were recorded in CH_2Cl_2 and acetonitrile solutions, respectively.

4. DISCUSSION

The experimental UV-vis spectrum measured for $[\text{Pt}(\text{tbtrpy})\text{OH}]\text{TCNQ}$ in CH_2Cl_2 solution has two pronounced bands in the low-energy region with peak maxima at 1.46 eV (851 nm)

and 1.65 eV (750 nm), respectively.⁹ A weaker transition appears at 1.62 eV (766 nm). The weak band with fine structure between 650 and 700 nm has its maximum at 1.81 eV (686 nm). $[\text{Pt}(\text{tbtrpy})\text{OH}]\text{TCNQ}$ in CH_2Cl_2 solution absorbs strongly below 550 nm with peak maxima at 2.52 eV (491 nm) and 3.06 eV (405 nm). A weak peak is also seen at 2.82 eV (440 nm). For the $[\text{Pt}(\text{tbtrpy})\text{Y}]^-$ complexes with $\text{Y} \neq \text{TCNQ}$ studied in ref 9, the strong absorption peaks in the low-energy region are missing because the counterions do not absorb in that energy range. At wavelengths shorter than 550 nm but in the visible range, the peaks originate from transitions to excited states of the $[\text{Pt}(\text{trpy})\text{OH}]^+$ cation, except for the small peak at 440 nm. The peak at 440 nm seems to be due to TCNQ^- , because it is missing in the spectrum when $\text{Y} \neq \text{TCNQ}$.⁹ Thus, the strong broad peak between 450 and 550 nm is most likely due to the low-energy transitions of the $[\text{Pt}(\text{trpy})\text{OH}]^+$ moiety. The exact position of the band depends on the X ligand and the electrostatic environment of the Y^- anion in the solution.

On the basis of the present calculations, the experimental spectra in Figure 1 might be explained in the following manner. The presence of the broad peak above 450 nm in the experimental spectrum indicates that the complex dissociates in solution. The exact position of the peak is determined by the Pt ligand (X). Thus, for the cases X, Y = Cl, Cl; X, Y = OH, BF_4^- ; and X, Y = NCS, BF_4^- the complexes studied in ref 9 are stable in solution rendering a blue shift of the peak, whereas the X, Y = CBT, Cl; X, Y = OH, TCNQ^- ; X, Y = PhS, BF_4^- ; and X, Y = DMBT, BF_4^- complexes dissociate.

The low-energy part of the electronic excitation spectrum of $[\text{Pt}(\text{trpy})\text{OH}]\text{TCNQ}$ calculated at the CC2 level has three dipole-allowed transitions, whereas in this energy range the experimental UV-vis spectrum is very reminiscent of the spectrum for the TCNQ^- anion.^{59,61,67} Thus, the calculated UV-vis spectrum for the $[\text{Pt}(\text{trpy})\text{OH}]\text{TCNQ}$ complex does not seem to correspond to the one measured in the CH_2Cl_2 solution implying that the $[\text{Pt}(\text{trpy})\text{OH}]^+$ and TCNQ^- ions are not forming any bound complex in the solvent. The measured spectrum is more or less a mixture of the individual UV-vis spectra of the $[\text{Pt}(\text{tbtrpy})\text{OH}]^+$ cation and the TCNQ^- anion, which apparently do not significantly perturb each other in the CH_2Cl_2 solution. Thus, the comparison of the calculated and measured spectra suggests that the $[\text{Pt}(\text{tbtrpy})\text{OH}]^+$ and TCNQ^- ions are dissolved and weakly interacting. In Figure 6, the simulated UV-vis spectrum for the $[\text{Pt}(\text{trpy})\text{OH}]\text{TCNQ}$ complex is compared with the combined simulated UV-vis spectra of $[\text{Pt}(\text{trpy})\text{OH}]^+$ and TCNQ^- , respectively. Chen et al. suggested that TCNQ^- is partially reduced to $\text{TCNQ}^{-(1+\delta)}$ in the $[\text{Pt}(\text{tbtrpy})\text{OH}]\text{TCNQ}$ complex.⁹ However, the model involving partial charges is not physically sound for dissociated ions.

5. CONCLUSIONS

The electronic excitation spectrum of neutral and charged TCNQ species, the $[\text{Pt}(\text{trpy})\text{OH}]^+$ cation, and the $[\text{Pt}(\text{trpy})\text{OH}]\text{TCNQ}$ complex have been studied at the CC2 and DFT levels using the linear-response approach. The calculated excitation energies and oscillator strengths are used for simulating UV-vis spectra, which are compared to measured ones. The calculated UV-vis spectrum for the $[\text{Pt}(\text{tbtrpy})\text{OH}]\text{TCNQ}$ complex is not in very close agreement with the experimental spectrum measured in CH_2Cl_2 solution, whereas the simulated UV-vis spectrum for an ionic mixture of the $[\text{Pt}(\text{tbtrpy})\text{OH}]^+$ cation and the TCNQ^- anion is much more

reminiscent of the recorded spectrum. The two spectra are compared in Figure 6. We therefore conclude that the [Pt(tbtrpy)OH]TCNQ complex is dissociated in CH_2Cl_2 .

■ ASSOCIATED CONTENT

S Supporting Information

Cartesian coordinates (in bohr) of the atoms of the studied molecules, excitation energies of the [Pt(tbtrpy)OH]TCNQ complex calculated at the B3LYP-COSMO level, electron-density plots for the highest occupied and lowest unoccupied Hartree-Fock orbitals, population analysis, atomic orbital contributions to the molecular orbitals, and atomic numbering diagrams are given as Supporting Information. This material is available free of charge via the Internet at <http://pubs.acs.org>.

■ AUTHOR INFORMATION

Corresponding Author

*D. Sundholm: e-mail, sundholm@chem.helsinki.fi.

Notes

The authors declare no competing financial interest.

[†]H. Rabaa: e-mail, hrabaa@yahoo.com.

[#]S. Taubert: e-mail, stefan.taubert@helsinki.fi.

■ ACKNOWLEDGMENTS

This research has been supported by the Academy of Finland through its Computational Science Research Programme (LASTU/258258) and projects (266227 and 268251). We thank Magnus Ehrnrooth Foundation for financial support. H.R. thanks the University of Helsinki for support. CSC-IT Center for Science is acknowledged for computer time.

■ REFERENCES

- (1) McMillin, D. R.; Moore, J. J. *Coord. Chem. Rev.* **2002**, *229*, 113–121.
- (2) Lippard, S. J. *Acc. Chem. Res.* **1978**, *11*, 211–217.
- (3) Lai, S.-W.; Chan, M. C. W.; Cheung, K.-K.; Che, C.-M. *Inorg. Chem.* **1999**, *38*, 4262–4267.
- (4) Willison, S. A.; Jude, H.; Antonelli, R. M.; Rennekamp, J. M.; Eckert, N. A.; Krause Bauer, J. A.; Connick, W. B. *Inorg. Chem.* **2004**, *43*, 2548–2555.
- (5) Aldridge, T. K.; Stacy, E. M.; McMillin, D. R. *Inorg. Chem.* **1994**, *33*, 722–727.
- (6) Kagan, C. R.; Mitzi, D. B.; Dimitrakopoulos, C. D. *Science* **1999**, *286*, 945–947.
- (7) Alonso, C.; Ballester, L.; Gutiérrez, A.; Perpiñán, M.; Sánchez, A.; Azcondo, M. *Eur. J. Inorg. Chem.* **2005**, *2005*, 486–495.
- (8) Rawashdeh-Omary, M. A.; Omary, M. A.; Fackler, J. P.; Galassi, R.; Pietroni, B. R.; Burini, A. *J. Am. Chem. Soc.* **2001**, *123*, 9689–9691.
- (9) Chen, W.-H.; Reinheimer, E. W.; Dunbar, K. R.; Omary, M. A. *Inorg. Chem.* **2006**, *45*, 2770–2772.
- (10) Smucker, B. W.; Hudson, J. M.; Omary, M. A.; Dubar, K. R. *Inorg. Chem.* **2003**, *42*, 4714–4723.
- (11) Rabaâ, H.; Cundari, T. R.; Omary, M. A. *Can. J. Chem.* **2009**, *87*, 775–783.
- (12) Klots, C. E.; Compton, R. N.; Raaen, V. F. *J. Chem. Phys.* **1974**, *60*, 1177–1178.
- (13) Compton, R. N.; Cooper, C. D. *J. Chem. Phys.* **1977**, *66*, 4325–4329.
- (14) Milián, B.; Pou-AméRigo, R.; Viruela, R.; Ortí, E. *Chem. Phys. Lett.* **2004**, *391*, 148–151.
- (15) Becke, A. D. *J. Chem. Phys.* **1993**, *98*, 5648–5652.
- (16) Lee, C.; Yang, W.; Parr, R. G. *Phys. Rev. B* **1988**, *37*, 785–789.
- (17) Andrae, D.; Häussermann, U.; Dolg, M.; Stoll, H.; Preuss, H. *Theor. Chim. Acta* **1990**, *77*, 123–141.
- (18) Schäfer, A.; Horn, H.; Ahlrichs, R. *J. Chem. Phys.* **1992**, *97*, 2571–2577.
- (19) Weigend, F.; Furche, F.; Ahlrichs, R. *J. Chem. Phys.* **2003**, *119*, 12753–12762.
- (20) Grimm, S.; Antony, J.; Ehrlich, S.; Krieg, H. *J. Chem. Phys.* **2010**, *132*, 154104.
- (21) Christiansen, O.; Koch, H.; Jørgensen, P. *Chem. Phys. Lett.* **1995**, *243*, 409–418.
- (22) Weigend, F.; Häser, M. *Theor. Chem. Acc.* **1997**, *97*, 331–340.
- (23) Hättig, C.; Weigend, F. *J. Chem. Phys.* **2000**, *113*, 5154–5161.
- (24) Köhn, A.; Hättig, C. *J. Chem. Phys.* **2003**, *119*, 5021–5036.
- (25) Hättig, C. *Adv. Quantum Chem.* **2005**, *50*, 37–60.
- (26) Casida, M. E. Time-dependent density-functional response theory for molecules. In *Recent Advances in Density Functional Methods, Part I*; Chong, D. P., Ed.; World Scientific: Singapore, 1995; pp 155–188.
- (27) Gross, E. K. U.; Dobson, J. F.; Petersilka, M. Density Functional Theory of Time-Dependent Phenomena. In *Density Functional Theory II*; Nalewajski, R. F., Ed.; Springer-Verlag: Berlin, 1996; Vol. 181, pp 81–172.
- (28) Bauernschmitt, R.; Ahlrichs, R. *Chem. Phys. Lett.* **1996**, *256*, 454–464.
- (29) Furche, F.; Ahlrichs, R. *J. Chem. Phys.* **2002**, *117*, 7433–7447.
- (30) Furche, F.; Ahlrichs, R. *J. Chem. Phys.* **2004**, *121*, 12772–12773.
- (31) Becke, A. D. *J. Chem. Phys.* **1993**, *98*, 1372–1377.
- (32) Yanai, T.; Tew, D. P.; Handy, N. C. *Chem. Phys. Lett.* **2004**, *393*, 51–57.
- (33) Dreuw, A.; Head-Gordon, M. *Chem. Rev.* **2005**, *105*, 4009–4037.
- (34) Wong, B. M.; Piacenza, M.; Sala, F. D. *Phys. Chem. Chem. Phys.* **2009**, *11*, 4498–4508.
- (35) Send, R.; Sundholm, D.; Johansson, M. P.; Pawłowski, F. *J. Chem. Theory Comput.* **2009**, *5*, 2401–2414.
- (36) Lehtonen, O.; Sundholm, D.; Send, R.; Johansson, M. P. *J. Chem. Phys.* **2009**, *131*, 024301.
- (37) Lehtonen, O.; Sundholm, D. *J. Chem. Phys.* **2006**, *125*, 144314.
- (38) Send, R.; Sundholm, D. *J. Phys. Chem. A* **2007**, *111*, 8766–8773.
- (39) Send, R.; Kaila, V. R. I.; Sundholm, D. *J. Chem. Phys.* **2011**, *134*, 214114.
- (40) Send, R.; Kaila, V. R. I.; Sundholm, D. *J. Chem. Theory Comput.* **2011**, *7*, 2473–2484.
- (41) Kaila, V. R. I.; Send, R.; Sundholm, D. *J. Phys. Chem. B* **2012**, *116*, 2249–2258.
- (42) Send, R.; Sundholm, D. *Phys. Chem. Chem. Phys.* **2007**, *9*, 2862–2867.
- (43) Schreiber, M.; Silva-Junior, M. R.; Sauer, S. P. A.; Thiel, W. *J. Chem. Phys.* **2008**, *128*, 134110.
- (44) Silva-Junior, M. R.; Schreiber, M.; Sauer, S. P. A.; Thiel, W. *J. Chem. Phys.* **2008**, *129*, 104103.
- (45) Gorelsky, S. I.; Lever, A. B. P. *J. Organomet. Chem.* **2001**, *625*, 187–196.
- (46) AOMix: Program for Molecular Orbital Analysis, version 6.82; 2013; <http://www.sg-chem.net/>.
- (47) Klamt, A.; Schüürmann, G. *J. Chem. Soc., Perkin Trans. 2* **1993**, 799–805.
- (48) Ahlrichs, R.; Bär, M.; Häser, M.; Horn, H.; Kölmel, C. *Chem. Phys. Lett.* **1989**, *162*, 165–169. Current version: see <http://www.turbomole.com>.
- (49) Frisch, M. J.; et al. *Gaussian 09*, Revision A.1; Gaussian Inc.: Wallingford, CT, 2009.
- (50) Hodges, M. P. *XMakemol: a program for visualizing atomic and molecular systems*, version 5.
- (51) Williams, T.; Kelley, C. *Gnuplot 4.5: an interactive plotting program*; 2011; <http://www.gnuplot.info/>.
- (52) VMD is developed with NIH support by the Theoretical and Computational Biophysics group at the Beckman Institute, University of Illinois at Urbana-Champaign, 1996.
- (53) Humphrey, W.; Dalke, A.; Schulten, K. *J. Mol. Graph.* **1996**, *14*, 33–38.

- (54) Laaksonen, L. A Graphics Program for the Analysis and Display of Molecular Dynamics Trajectories. *J. Mol. Graph.* **1992**, *10*, 33–34.
- (55) Bergman, D. L.; Laaksonen, L.; Laaksonen, A. Visualization of Solvation Structures in Liquid Mixtures. *J. Mol. Graph. Modelling* **1997**, *15*, 301–306.
- (56) Allen, F. H. *Acta Crystallogr. B* **2002**, *58*, 380–388.
- (57) Jonkman, H. T.; Kommandeur, J. *Chem. Phys. Lett.* **1972**, *15*, 496–499.
- (58) Zanon, I.; Pecile, C. *J. Phys. Chem.* **1983**, *87*, 3657–3664.
- (59) Roberts, G. M.; Lecointre, J.; Horke, D. A.; Verlet, J. R. *R. Phys. Chem. Chem. Phys.* **2010**, *12*, 6226–6232.
- (60) Gorishnyi, M. P. *Ukr. J. Phys.* **2004**, *49*, 1158–1162.
- (61) Jeanmaire, D. L.; Van Duyne, R. P. *J. Am. Chem. Soc.* **1976**, *98*, 4029–4033.
- (62) Dierksen, M.; Grimme, S. *J. Phys. Chem. A* **2004**, *108*, 10225–10237.
- (63) Makowski, M.; Pawlikowski, M. T. *Int. J. Quantum Chem.* **2006**, *106*, 1736–1748.
- (64) Dunning, T. H., Jr. *J. Chem. Phys.* **1989**, *90*, 1007–1023.
- (65) Skurski, P.; Gutowski, M. *J. Mol. Struct.: THEOCHEM* **2000**, *531*, 339–348.
- (66) Pyykkö, P.; Atsumi, M. *Chem.—Eur. J.* **2009**, *15*, 186–197.
- (67) Li, Z.-J.; Li, Z.-R.; Wang, F.-F.; Ma, F.; Chen, M.-M.; Huang, X.-R. *Chem. Phys. Lett.* **2009**, *468*, 319–324.